



HAL
open science

Mixed valence (μ -phenoxido) $\text{Fe}^{II}\text{Fe}^{III}$ and $\text{Fe}^{III}\text{Fe}^{IV}$ compounds: Electron and proton transfers

Patrick Dubourdeaux, Geneviève Blondin, Jean-Marc Latour

► **To cite this version:**

Patrick Dubourdeaux, Geneviève Blondin, Jean-Marc Latour. Mixed valence (μ -phenoxido) $\text{Fe}^{II}\text{Fe}^{III}$ and $\text{Fe}^{III}\text{Fe}^{IV}$ compounds: Electron and proton transfers. *ChemPhysChem*, 2022, 23 (2), pp.e202100399. 10.1002/cphc.202100399 . hal-03535148

HAL Id: hal-03535148

<https://hal.science/hal-03535148v1>

Submitted on 15 Nov 2022

HAL is a multi-disciplinary open access archive for the deposit and dissemination of scientific research documents, whether they are published or not. The documents may come from teaching and research institutions in France or abroad, or from public or private research centers.

L'archive ouverte pluridisciplinaire **HAL**, est destinée au dépôt et à la diffusion de documents scientifiques de niveau recherche, publiés ou non, émanant des établissements d'enseignement et de recherche français ou étrangers, des laboratoires publics ou privés.

Mixed valence (μ -phenoxido) $\text{Fe}^{\text{II}}\text{Fe}^{\text{III}}$ et $\text{Fe}^{\text{III}}\text{Fe}^{\text{IV}}$ compounds: electron and proton transfers

Patrick Dubourdeaux,^[a] Geneviève Blondin^[a] and Jean-Marc Latour*^[a]

Dedication This mini-review is dedicated to the memory of Prof. Dr. Jean-Michel Savéant.

[a] P. Dubourdeaux, Dr G. Blondin, Dr J.-M. Latour
 [a] Univ. Grenoble Alpes, CEA, CNRS, IRIG- LCBM / pmb, F-38000 Grenoble, France
 E-mail: jean-marc.latour@cnsr.fr.

Abstract: Mixed-valence non heme diiron centers are present at the active site of a few enzymes and confer them interesting reactivities with the two ions acting in concert. Related (μ -phenoxido)diiron complexes have been developed as enzyme mimics. They exhibit very rich spectroscopic properties enabling independent monitoring of each individual ion, which proved useful for mechanistic studies of catalytic hydrolysis and oxidation reactions. In our studies of such complexes, we observed that these compounds give rise to a wide variety of electron transfers (intervalence charge transfer), proton transfers (tautomerism), coupled electron and proton transfers (H^+ abstraction and PCET). In this minireview, we present and analyze the main results illustrating the latter aspects.

1. Introduction

Non heme diiron proteins are well known for their involvement in dioxygen transport and metabolism in a plethora of organisms.^[1,2] They generally operate through homovalent iron pairs: $\text{Fe}^{\text{II}}\text{Fe}^{\text{II}}$, $\text{Fe}^{\text{III}}\text{Fe}^{\text{III}}$ and $\text{Fe}^{\text{IV}}\text{Fe}^{\text{IV}}$. By contrast, a limited number of them, mammalian purple acid phosphatases (mPAP)^[3] and myoinositol oxygenases (MIOX),^[4] rely on the mixed-valence state $\text{Fe}^{\text{III}}\text{Fe}^{\text{II}}$ for their hydrolytic and oxidative functions, respectively. In both types of enzymes, the irons are bound to O/N ligands and are bridged by a hydroxido ion (Figure 1).^[5–8] Their unsaturated coordination sphere allows them to bind their substrate. Purple acid phosphatases owe their name to the presence of a terminal tyrosinate bound to the Fe^{III} ion which contributes a strong charge transfer absorption $\text{Tyr} \rightarrow \text{Fe}^{\text{III}}$. They belong to the family of dimetal hydrolases which catalyze the hydrolysis of a wealth of biological phosphate esters.^[9] Depending on their origin, they rely on different $\text{Fe}^{\text{III}}\text{M}^{\text{II}}$ couples where the second metal M can be either Mn, Fe or Zn. The Fe_2 enzymes, which are found in mammals, have received special attention from a medicinal point of view.^[10–12] Their mechanism of action has been investigated in detail both on the enzymes^[3] and on synthetic model complexes.^[13,14] It is generally admitted that the Fe^{II} center Fe_B in Figure 1(a) binds the substrate through a phosphate oxygen and the Fe^{III} center Fe_A binds a hydroxido ion in an adequate orientation to attack the P atom of the phosphate. MIOX is one of the very few enzymes which use an Fe-bound superoxide to oxidize its substrate.^[15] To achieve it, the mixed-valence $\text{Fe}^{\text{III}}\text{Fe}^{\text{II}}$ enzyme activates dioxygen to form a superoxo $\text{Fe}^{\text{III}}\text{Fe}^{\text{III}}$ species which performs an H^+ abstraction from Fe^{III} -bound myoinositol.^[4]

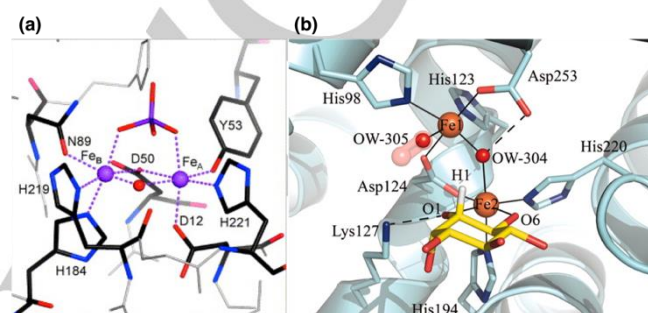
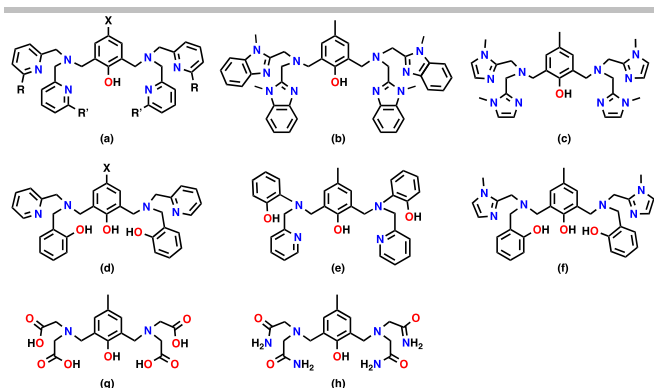


Figure 1. X-ray structures of the active sites of (a) recombinant human Purple Acid Phosphatase bound to phosphate anion^[7] and (b) MIOX bound to myoinositol (highlighted in yellow).^[8]

Most studies of these enzymes took advantage of the very rich physical and spectroscopic properties of the $\text{Fe}^{\text{III}}\text{Fe}^{\text{II}}$ pair.^[16–19] As a matter of fact, each ion can be monitored individually by several spectroscopic techniques, while, owing to the presence of a hydroxido bridge, the two ions constitute a mixed-valence pair with specific physical properties. These features are present also in (μ -phenoxido)diiron model compounds. We have exploited them as part of a general interest in mixed-valence species^[20,21] and for in depth mechanistic studies of phosphate ester hydrolysis^[14] and nitrene^[22–24] transfer reactions. In the course of these studies, various types of proton and electron transfers have emerged: intervalence transfer, tautomerism, H^+ abstraction and proton-coupled intervalence transfer that we studied in collaboration with J.-M. Savéant and his group.^[25] It is the purpose of this minireview to survey all these processes. The various types of binucleating phenol ligands and the general syntheses of the diiron complexes will be exposed first (Section 2). The valence location and intervalence transfer of the complexes will then be analyzed with the help of a wealth of spectroscopic techniques (Section 3). After presentation of their redox properties (Section 4), electron and proton transfers will be considered (Section 5). Finally, the H^+ abstraction reactions and a tautomerism of high-valent imidodiiron species will be described (Section 6), before highlighting some most salient features (Section 7).

MINIREVIEW



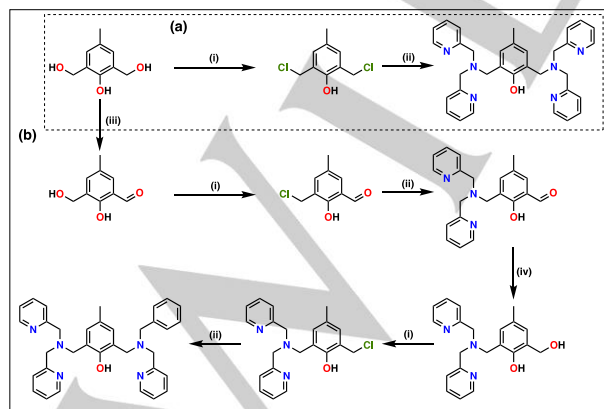
Scheme 1. Symmetrical ligands: (a) HXL[(R'Py)(R'Py)][(R'Py)(R'Py)] with R=R'=H and X=Me,^[26] OMe^[27] and tBu,^[28] and R=H, R'=Me and X=Me^[29] or NO₂,^[30] (b) HL[(MeBzIm)₂][(MeBzIm)₂],^[31,32] (c) HL[(Melm)₂][(Melm)₂],^[33] (d) HXL[(Py)(BnOH)][(Py)(BnOH)] with X=Me,^[34] tBu,^[35] (e) HL[(Py)(PhOH)][(Py)(PhOH)],^[36] (f) HL[(Melm)(BnOH)][(Melm)(BnOH)],^[37] (g) HL[(AcOH)₂][(AcOH)₂],^[38,39] (h) HL[(AcNH₂)₂][(AcNH₂)₂].^[40]

2. Binucleating Phenol Ligands and Synthesis of (μ-phenoxido) Diiron Complexes

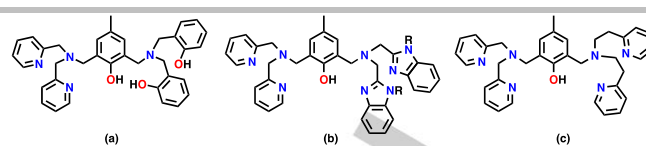
2.1. Ligands Syntheses

Initial studies of (μ-phenoxido)diiron complexes were based on symmetrical ligands associating with the bridging phenol four identical complexing groups, i.e. carboxylates,^[41] 2-pyridyl,^[42] 2-imidazolyl^[33] and 2-benzimidazolyl^[32] (Scheme 1a-c and g). The various abbreviations used over the years by different groups do not allow an immediate access to the composition of the ligands. To access it readily, we have renamed them in a systematic manner specifying the two donors within the two complexing branches. Whereas most of the ligands involve a *p*-methyl substituent on the phenol, in a few cases (Scheme 1a and d) other substituents were used (i.e. OMe and tBu). For these specific ligands the para substituent will be specified, while for the others the methyl will be omitted.

Later, mixed amine/phenol branches were introduced to mimic the tyrosinate ligand present in mPAP (Scheme 1d-f).^[34,36,37,43] All these symmetrical ligands are easily accessible through condensation of two equivalents of the lateral diamine or



Scheme 2. Main general synthetic routes to access representative symmetrical HL[(Py)₂][(Py)₂]^[26] (a) and unsymmetrical HL[(Py)₂][(Py)(Bn)]^[21] (b) ligands. Conditions: (i) SOCl₂/CH₂Cl₂, (ii) bis-picolylamine/NEt₃, (iii) MnO₂/toluene, (iv) NaBH₄/THF.



Scheme 3. Unsymmetrical ligands HL[(Py)₂][(D)₂] with D = 2-hydroxybenzyl,^[44] benzimidazolyl (R=H or Me),^[45] or 2-(2-pyridyl)ethyl.^[46]

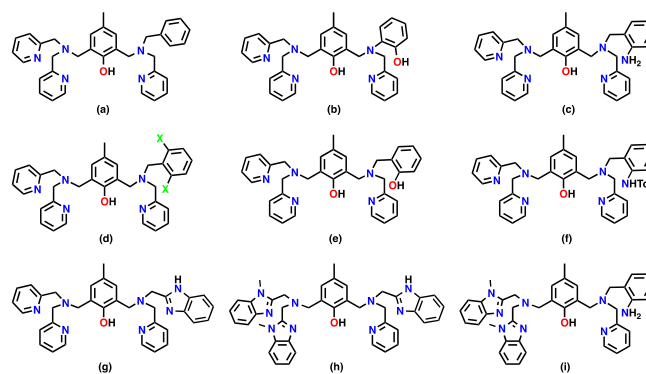
amine/phenol branch to the central platform 2,6-bis-(chloromethyl)phenol (Scheme 2a), obtained by chlorination of the commercially available 2,6-bis-(hydroxymethyl)phenol.

Various unsymmetrical ligands harboring different lateral branches were also designed for specific purposes. A few of them associate a bis-picolylamine branch and another bis-substituted one (Scheme 3).^[44,46,47]

To more closely mimic the binding pattern of mPAP which provides a single terminal tyrosinate ligand, unsymmetrical ligands were designed (Scheme 4b, e) which bear a phenol group on a single branch.^[48] The above synthetic method provides a mixture of ligands from which the targeted one must be separated by chromatography, which results in low yields.^[49] A specific synthesis is obviously less straightforward because it requires to anchor the two different branches sequentially after making the phenol platform unsymmetrical through selective oxidation of one hydroxymethyl function (Scheme 2b).^[48,50] The same chlorination/alkylation sequence of reactions was used to introduce different other donors and even insert a vacant coordination site on a single iron (as found in the dioxygen carrier hemerythrin)^[51] which allows the binding of reagents (Scheme 4a and d).^[20]

2.2. Syntheses of Diiron Complexes

The synthesis of the diiron complexes is straightforward: reaction of the ligand (possibly in the presence of a base to deprotonate the phenol) with 2 equivalents of iron salts in the presence of 2 equivalents of a suitable μ-1,3-bridging group. The latter is generally a carboxylate but a phosphate ester^[27,43,52] or even the sulfate dianion^[53] have been used also. A dicarboxylate, *m*-phenylenedipropionate (mpdp²⁻),^[54] has been used also to further stabilize the diiron unit in certain instances.^[20]



Scheme 4. Unsymmetrical ligands HL[(Py)₂][(Py)(D)] (with D = benzyl (a), 2-hydroxyphenyl^[48] (b), 2-aminobenzyl^[47] (c), 2,6-dichlorobenzyl^[55] (d), 2-hydroxybenzyl^[21,49] (e), 2-tosylaminobenzyl^[22] (f) and 2-benzimidazolyl^[45] (g), and HL[(MeBzIm)₂][(Py)(D)] (with D = 2-benzimidazolyl^[45] (h) and 2-aminobenzyl^[45] (i)).

MINIREVIEW

Depending on the ligand and on the complexation conditions, the diiron unit can be isolated in various oxidation states $\text{Fe}^{\text{II}}\text{Fe}^{\text{II}}$, $\text{Fe}^{\text{II}}\text{Fe}^{\text{III}}$, $\text{Fe}^{\text{III}}\text{Fe}^{\text{III}}$. Strict anaerobic conditions are required to prepare the reduced $\text{Fe}^{\text{II}}\text{Fe}^{\text{II}}$ complexes.^[41,56] By contrast, the mixed-valence and oxidized forms can be obtained in air where their stability depends on the nature of the ligation within the lateral branches: the mixed-valence form $\text{Fe}^{\text{II}}\text{Fe}^{\text{III}}$ is favored when these branches contain only nitrogen donors. They can be obtained by anaerobic reaction of the ligand with a ferrous salt, which gives the diferrous complex $\text{Fe}^{\text{II}}\text{Fe}^{\text{II}}$, followed by air oxidation.^[32,42] Alternatively, they can be obtained by reaction of the ligand in methanol with a ferric salt, producing the diferric complex $\text{Fe}^{\text{III}}\text{Fe}^{\text{III}}$ which is reduced by the solvent.^[57,58] When the ligands possess several phenolic donors and favor the bis-ferric state, the mixed-valence species could be generated by its one-electron reduction.

Higher valences of the diiron pair have been evidenced during oxidation reactions. As a matter of fact, two intermediates in nitrene transfer processes have been assigned the electronic structures $\text{Fe}^{\text{III}}\text{Fe}^{\text{IV}} \leftrightarrow [\text{Fe}^{\text{III}}\text{Fe}^{\text{III}}\text{NTs}]^{2+}$ and $[\text{Fe}^{\text{III}}\text{Fe}^{\text{IV}}\text{NTs}]^{2+}$.^[24] These high valent species are too elusive to be isolated and have been detected and identified by Desorption ElectroSpray Ionization thanks to ^{15}N labeling (See Section 6).

3. Valence location in mixed-valent (μ -phenoxido) $\text{Fe}^{\text{II}}\text{Fe}^{\text{III}}$ complexes

Owing to their specific electronic structures, mixed-valent $\text{Fe}^{\text{II}}\text{Fe}^{\text{III}}$ complexes exhibit very rich spectroscopic and magnetic properties which offer many ways to investigate them. One major interest in their electronic structures is the possibility of a valence inversion between the two Fe sites, leading to the questions of the location of these valences and the rate of their inversion.

These questions have been addressed within the framework of Robin and Day classification^[59] of mixed-valence compounds, using on particular the formalism developed by Hush.^[60] These studies will be presented in Sections 3.3-3.5 for the complex $\{\text{L}[(\text{Py})_2][(\text{Py})_2]\text{Fe}^{\text{II}}(\text{EtCO}_2)_2\text{Fe}^{\text{III}}\}^{2+}$ (Figure 2a). As a preamble to describing these features, we present in the next two sections their structural and magnetic properties.

3.1. Structures of $\text{Fe}^{\text{II}}\text{Fe}^{\text{III}}$ Mixed-Valence Complexes

The X-ray structures of a dozen (μ -phenoxido) $\text{Fe}^{\text{II}}\text{Fe}^{\text{III}}$ compounds have been determined (Figure 2).^[20,27,28,33,45,47,48,58,61-63] Most exhibit a triply bridged core $[\text{Fe}^{\text{II}}(\mu\text{-PhO})(\mu\text{-RCO}_2)_2\text{Fe}^{\text{III}}]$ (R = Me, Et or Ph). The Fe ions are bound by oxygen and nitrogen ligands in octahedral environments. In spite of different lateral coordination sets, they reveal quite similar features attesting that the valences of the two ions are localized in the solid state, even for complexes with identical donor sets in the two branches.^[33,58] Indeed, significantly different $\text{Fe-O}_{\mu\text{-ph}}$ distances ($\text{O}_{\mu\text{-ph}}$ is the bridging phenoxido oxygen) are noted which clearly identify the ferrous and ferric sites: $\text{Fe}^{\text{II}}\text{-O}_{\mu\text{-ph}}$ 2.07 - 2.17 Å and $\text{Fe}^{\text{III}}\text{-O}_{\mu\text{-ph}}$ 1.94 - 1.96 Å. The Fe-Fe distances and the $\text{Fe-O}_{\mu\text{-ph}}\text{-Fe}$ angles are confined within a narrow range from 3.36 to 3.48 Å and from 108 to 120°, respectively. Replacement of the carboxylato bridges by diphenylphosphate leads to increasing both the Fe-Fe distance and the $\text{Fe-O}_{\mu\text{-ph}}\text{-Fe}$ angle to 3.64 Å and 121.4°, respectively.^[27,43,52]

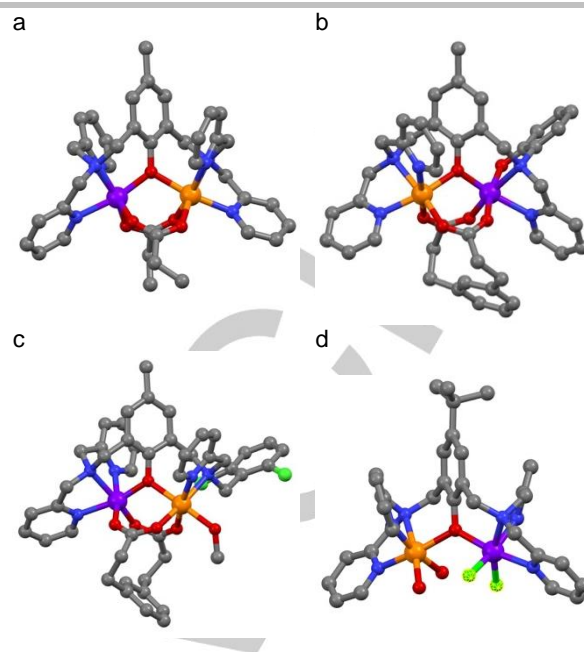


Figure 2. X-ray structures of the cations $\{\text{L}[(\text{Py})_2][(\text{Py})_2]\text{Fe}^{\text{II}}(\text{EtCO}_2)_2\text{Fe}^{\text{III}}\}^{2+}$ (a), $\{\text{L}[(\text{Py})_2][(\text{Py})(\text{PhO})]\text{Fe}^{\text{II}}(\text{mpdp})\text{Fe}^{\text{III}}\}^+$ (b), $\{\text{L}[(\text{Py})_2][(\text{Py})(\text{BnCl}_2)]\text{Fe}^{\text{III}}(\text{mpdp})\text{Fe}^{\text{II}}(\text{MeOH})\}^{2+}$ (c) and $\{\text{BuL}[(\text{Py})_2][(\text{Py})_2]\text{Fe}^{\text{II}}(\text{OH})_2\text{Fe}^{\text{III}}\}^{2+}$ (d). mpdpH₂ is *m*-phenylene dipropionic acid. Color code: Fe^{II} in orange, Fe^{III} in purple.

This is probably due to the enlarged bite angle of diphenylphosphate vs carboxylate and will affect the electronic properties of the Fe_2 core (See below). A single complex was reported with only the phenoxido bridge, the Fe coordination spheres being completed by water molecules and fluoride ligands (Figure 2d). Even larger Fe-Fe distance (3.73 Å) and $\text{Fe-O}_{\mu\text{-ph}}\text{-Fe}$ angle (124.6°) values were noted.^[61]

3.2. Magnetic properties and EPR of $\text{Fe}^{\text{II}}\text{Fe}^{\text{III}}$ Mixed-Valence Complexes

The heptadentate ligand and the two extra carboxylate bridges provide high-spin electronic configurations to the metal ions. Variations of the molar magnetic susceptibility with the temperature were well-interpreted by assuming localized valences. The data revealed a weak antiferromagnetic interaction between the $S_A=2$ ferrous ion and the $S_B=5/2$ ferric ion, leading to a $S=1/2$ ground state. The antiferromagnetic exchange interaction lies between 6.4 and 16.0 cm^{-1} ($H_{\text{HDVV}}=J S_A \cdot S_B$).^[32,42,48,49] More thorough analyses have also included the zero-field splitting effect of the ferrous ion that is indeed of similar magnitude compared with the exchange interaction.^[33,21,29,62] Changing carboxylates into phosphates leads to similar exchange interactions.^[21,64] However, replacing the two carboxylates bridges by a methoxide led to an increase of J to 26 cm^{-1} .^[44] The $S=1/2$ ground state was confirmed by X-band EPR spectroscopy. The observed signals were characterized by averaged g -values below 2, which is fully consistent with the antiferromagnetic coupling between a high-spin (^6A state) Fe^{III} ion and a high-spin (^5T state) Fe^{II} ion. It should be noted that these signals are often quite broad and their detection requires very low temperatures, below 20 K or even below 4 K.^[13,16,29,32,42,58] This situation results from the comparable values of the small exchange coupling and the zero-field splitting

MINIREVIEW

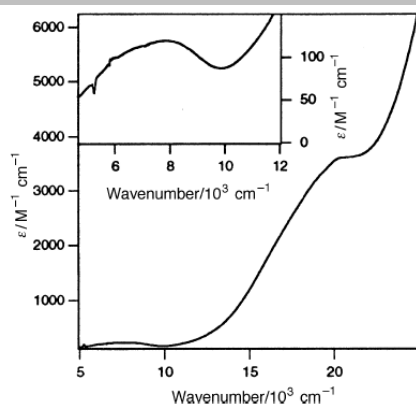


Figure 3. Absorption spectrum of $\{L[(Py)_2]_2[(Py)_2]Fe^{III}(EtCO_2)_2Fe^{II}\}^{2+}$ in acetone solution. The inset shows the intervalence band in CD_3CN .^[65]

of the ferrous site^[21] (See above), as found for reduced pig purple acid phosphatase (uteroferrin).^[66]

3.3. UV-visible spectroscopy

As for most ferric phenoxides, the UV-visible spectra of $(\mu\text{-phenoxido})Fe^{II}Fe^{III}$ compounds are dominated by an intense phenoxide to Fe^{III} charge transfer in the visible region (around 500 - 600 nm). But as a distinctive feature, they exhibit in the near infra-red region (7000 - 10000 cm^{-1}) an absorption with a low extinction coefficient (60 - 310 $M^{-1} cm^{-1}$) which has been assigned to an intervalence transition (IVT).^[29,32,33,42,49,58] Based on the pioneering work of N. S. Hush^[60], Que and his group^[39] were able to evaluate the delocalization coefficient, that is the mixing of oxidation states, for complex $\{L[(Py)_2]_2[(Py)_2]Fe^{III}(EtCO_2)_2Fe^{II}\}^{2+}$. Weak values were determined, typically lower than 0.01. In addition, the rate of electron exchange was evaluated to ca 2×10^{12} Hz. It is worth noting that these bands are present whatever the symmetrical^[16,29,32,33,42,58] or unsymmetrical^[21,49] nature of the ligand, pointing in all cases to some electronic delocalization.

Analogous intervalence bands were detected on polycrystalline samples.^[67] As a matter of fact, Reber et al.^[65] studied the same compound in solid state from 6 K to room temperature. The intensity of the IVT was very weak at 6 K but increased with a rise in temperature, in agreement with a vibronic intensity mechanism. Time-dependent calculations using one configurational coordinate with a non-constant transition dipole moment along this coordinate adequately reproduced the energy and the temperature dependence of the intervalence band.

Robert and coworkers^[68] developed a detailed computational analysis of the intervalence transfer of the complex $\{L[(Py)_2]_2[(Py)(BnNH_2)]Fe^{III}(mpdp)Fe^{II}\}^{2+}$. Using state-average CASSCF calculations, they showed that the electronic reorganization is the major contributor to the reorganization energy of the IVT transition. In addition, their calculations revealed that this large effect is produced by a relatively small adaptation of the Fe valence electrons, especially from the pyridine ligands.

3.4. Mössbauer spectroscopy

^{57}Fe -Mössbauer spectroscopy recorded on polycrystalline samples was extensively used to characterize $(\mu\text{-phenoxido})Fe^{II}Fe^{III}$ complexes.

At 80 K or below, all detected spectra are composed of two doublets in a close to 1:1 ratio (Figure 4, bottom spectrum).^[20,21,32,42,58,69] The nuclear parameters of the first doublet are characteristic of a high-spin ferrous ion in a O/N environment with isomer shift lying between 1.07 and 1.29 $mm s^{-1}$ and quadrupole splitting between 2.06 and 3.24 $mm s^{-1}$. The second doublet presents smaller isomer shift (0.43 - 0.58 $mm s^{-1}$) and quadrupole splitting (0.31 - 0.96 $mm s^{-1}$). These values are fully consistent with a high-spin ferric ion in an octahedral environment. Accordingly, Mössbauer spectra at 80 K revealed localized valences. However, for some complexes of symmetrical ligands $HL[(Py)_2]_2[(Py)_2]$ and $HL[(Melm)_2]_2[(Melm)_2]$ (Scheme 1a and c, respectively), Mössbauer spectra recorded at higher temperatures up to 330 K evidenced more or less important changes which revealed different behaviors (Figure 4).^[33,67,69,70] In some systems, increasing the temperature leads the two doublets to shift with a significant broadening.^[67] They may merge in a unique one with nuclear parameter values intermediate between those of ferrous and ferric ions.^[69,70] This behavior suggests an electron hopping between the two iron sites with a rate comparable to the inverse Mössbauer time scale ($\approx 10^2$ MHz). The temperature dependence of these Mössbauer spectra has been analyzed in detail, considering that the extra electron stays a little longer on one site versus the other.^[67] A 80:20 ratio between the two electronic configurations $Fe^{II}_A Fe^{III}_B$ and $Fe^{III}_A Fe^{II}_B$ gives satisfying simulations of the Mössbauer spectra. In addition, a 15-25 $kJ mol^{-1}$ activation barrier for the electron transfer was determined from the temperature dependence of the electron hopping frequency.^[67,70]

In other complexes, Mössbauer spectra evidenced a third doublet in addition to those associated with the ferrous and ferric ions.^[33,71] This third doublet has been associated with a fully delocalized mixed-valence species, namely $Fe^{2.5+}Fe^{2.5+}$, with an increasing contribution as the temperature is increased from 100 to 300 K, indicating an electron transfer rate exceeding the Mössbauer time scale. Reported studies evidenced that the electron hopping behavior is moderately influenced by electronic factors (nature of the heptadentate ligand and the carboxylate bridges). Crystal packing modifications due to changes in counter ions and carboxylates appear responsible for the diverse behaviors observed but no further rationalization was advanced

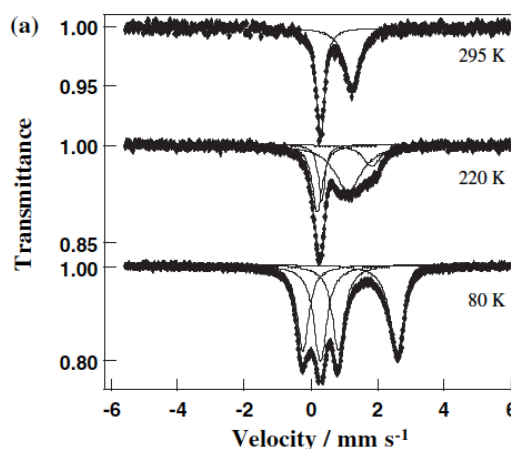


Figure 4. Mössbauer spectra of complex $\{L[(Py)_2]_2[(Py)_2]Fe^{III}(C_6H_{13}CO_2)_2Fe^{II}(ClO_4)_2\}^{7/2+}$. The hash bars are the experimental spectra and the thin line represents the theoretical contributions of the Fe ions at each temperature.

MINIREVIEW

3.5. ^1H NMR spectroscopy

$(\mu\text{-phenoxido})\text{Fe}^{\text{II}}\text{Fe}^{\text{III}}$ complexes possess well resolved ^1H NMR spectra extending over very large spectral ranges up to 600 ppm. These features result from a combination of specific electronic properties: (i) the fast electronic relaxation of the Fe^{II} ion adopted by the complex, and (ii) the strong paramagnetism of the complex due to the weak magnetic interaction between the two Fe centers.^[58] Full assignment of the ^1H NMR spectrum of $\{\text{L}[(\text{Py})_2][(\text{Py})_2]\text{Fe}^{\text{III}}[\text{O}_2\text{P}(\text{OPh})_2]_2\text{Fe}^{\text{II}}\}^{2+}$ was achieved by the group of Que^[56] and led to attribute the most downfield shifted signal at 370 ppm to the benzyl proton more "in-plane" with the Fe binding motif and the most upfield shifted one at 3.8 ppm to a picolyl methylene proton. Electron hopping in this complex is evidenced by several features: (i) the number of peaks is ca halved vs the number of protons revealing an effective 2-fold symmetry of the molecule, and (ii) the most downfield shifted resonance for the same proton in the bis-ferrous analog $\{\text{L}[(\text{Py})_2][(\text{Py})_2]\text{Fe}^{\text{II}}[\text{O}_2\text{P}(\text{OPh})_2]_2\text{Fe}^{\text{II}}\}^+$ appears at a negative shift -33.8 ppm, revealing an averaging of the resonances in the mixed-valent analog. The rate of intramolecular electron transfer was estimated $>10^5 \text{ s}^{-1}$.^[56] A similar behavior was observed for other complexes of symmetrical ligands.^[33,57,58] By contrast, when the ligand is unsymmetrical, albeit closely related as $\text{HL}[(\text{Py})_2][(\text{Py})(\text{Bn})]$ (Scheme 4a), the valences of the mixed-valent complex $\{\text{L}[(\text{Py})_2][(\text{Py})(\text{Bn})]\text{Fe}^{\text{III}}(\text{mpdp})\text{Fe}^{\text{II}}(\text{NCCH}_3)\}^{2+}$ become localized as evidenced by the different temperature dependences of the resonances of protons close to the Fe^{II} vs Fe^{III} ion.^[20] In addition, the spectral range is hugely enlarged (>600 ppm) since the two above mentioned resonances occur at 560 and -50 ppm, respectively.^[21,47,62,63] A switch from a partly delocalized to a localized situation was evidenced for complexes of unsymmetrical ligands possessing protic N donors in the branches (Schemes 3b, 4c and g-i).^[45]

For instance, deprotonation of the benzimidazole in the lateral branch of $\{\text{L}[(\text{MeBzIm})_2][\text{BzImH}]_2\text{Fe}^{\text{III}}(\text{mpdp})\text{Fe}^{\text{II}}\}^{2+}$ induces a full localization of the Fe valences. As a matter of fact, the resonances close to the Fe^{II} ion (see for instance peak B in Figure 5) move upfield as opposed to those close to Fe^{III} which move downfield (see for instance peak A in Figure 5), thereby leading to an enlarged spectrum.

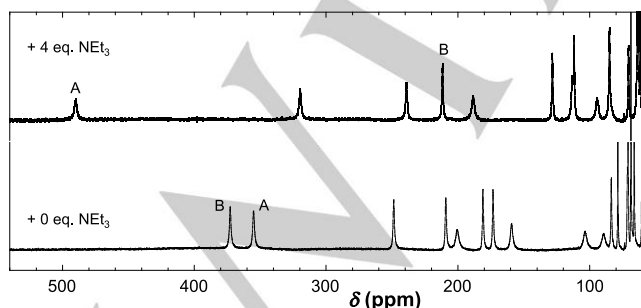


Figure 5. NMR spectra of CD_3CN solution of $\{\text{L}[(\text{Py})_2][(\text{BzImH})_2]\text{Fe}^{\text{III}}(\text{mpdp})\text{Fe}^{\text{II}}\}^{2+}$ in absence (bottom) and in presence (top) of 4 eq. NEt_3 . Peaks A and B correspond to the "in-plane" proton of the $\text{N-CH}_2\text{-PhO}^-$ group coordinated to the ferric and ferrous ion, respectively.^[45]

In addition to the dependence on the electron delocalization, the chemical shift is also highly sensitive to the magnitude of the antiferromagnetic exchange interaction between the two metallic sites: the less shifted, the stronger the coupling. This behavior was evidenced in our studies of the mechanism of phosphate ester hydrolysis. The ^1H NMR spectrum of the complex $\{\text{L}[(\text{Py})_2][(\text{Py})(\text{Bn})]\text{Fe}^{\text{III}}(\text{OAc})_2\text{Fe}^{\text{II}}(\text{NCCH}_3)\}^{2+}$ in CD_3CN extends over 573 ppm (from 540 to -33 ppm). Addition of 25 % D_2O induced a moderate shrinking of the spectral range to 514 ppm (from 500 to -14 ppm) assigned to loss of a carboxylate bridge which is a poor mediator of antiferromagnetic exchange. By contrast, addition of sodium hydroxide, providing a hydroxido bridge which is a moderate mediator, caused a dramatic contraction to 229 ppm (from 217 to -12 ppm).^[14]

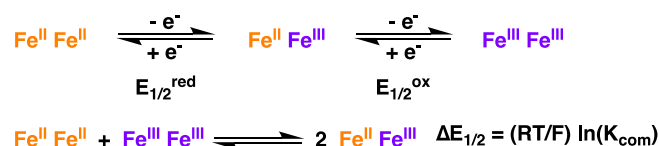
3.6. Mixed-valent character

To summarize the above spectroscopic studies, when the ligands provide the two Fe sites with similar coordination spheres (Schemes 1, 3b,c and 4a,c,d,g-i) as detailed in Sections 3.3 - 3.5 for the complex $\{\text{L}[(\text{Py})_2][(\text{Py})_2]\text{Fe}^{\text{III}}(\text{EtCO}_2)_2\text{Fe}^{\text{II}}\}^{2+}$ (Figure 2a), these $(\mu\text{-phenoxido})\text{Fe}^{\text{II}}\text{Fe}^{\text{III}}$ complexes are typical class II examples according to the Robin and Day classification^[59] of mixed-valence compounds. However, they rapidly tend to localize when even a small unsymmetry is introduced.

4. Redox Potentials and Stability Domains of $(\mu\text{-Phenoxido})\text{Fe}^{\text{II}}\text{Fe}^{\text{III}}$ Complexes4.1. Redox Potentials of $(\mu\text{-Phenoxido})\text{Fe}^{\text{II}}\text{Fe}^{\text{III}}$ Complexes

$(\mu\text{-phenoxido})\text{Fe}^{\text{II}}\text{Fe}^{\text{III}}$ complexes can be both reduced and oxidized to their homovalent $\text{Fe}^{\text{II}}\text{Fe}^{\text{II}}$ and $\text{Fe}^{\text{III}}\text{Fe}^{\text{III}}$ counterparts, respectively (Scheme 5). The electrochemical potentials of these one-electron transfers ($E_{1/2}^{\text{red}}$ and $E_{1/2}^{\text{ox}}$) are strongly dependent on the donating groups within the lateral branches. When the branches associate four N donors as in ligand $\{\text{HL}[(\text{Py})_2][(\text{Py})_2]\}$ (Scheme 1a-c, Scheme 3b,c and Scheme 4g,h), $E_{1/2}^{\text{red}}$ and $E_{1/2}^{\text{ox}}$ values cluster in a narrow range $-0.06 \pm 0.12 \text{ V}_{\text{sce}}$ and $+0.60 \pm 0.13 \text{ V}_{\text{sce}}$, respectively. Hence, the mixed-valent form is the stable one in aerobic conditions. When each branch incorporates both a N and an anionic O donor as in ligand $\{\text{HL}[(\text{Py})(\text{BnO})][(\text{Py})(\text{BnO})]\}$ (Scheme 1d-f), the values of these potentials are strongly shifted negatively ($E_{1/2}^{\text{red}} = -0.83 \pm 0.09 \text{ V}_{\text{sce}}$ and $E_{1/2}^{\text{ox}} = -0.17 \pm 0.03 \text{ V}_{\text{sce}}$). The potential shift amounts to -770 mV for both potentials, which shows that the $\text{Fe}^{\text{II}}\text{Fe}^{\text{III}}$ pair behaves as a redox unit sensitive to its overall charge.

Quite expectedly, intermediate values are found for the corresponding electrochemical potentials of the complexes possessing a single anionic donor in one branch as in ligand $\{\text{HL}[(\text{Py})_2][(\text{Py})(\text{BnO})]\}$ (Scheme 4b,e) ($E_{1/2}^{\text{red}} = -0.55 \pm 0.05 \text{ V}_{\text{sce}}$ and $E_{1/2}^{\text{ox}} = 0.37 \pm 0.04 \text{ V}_{\text{sce}}$). Nevertheless, the reduction and



Scheme 5. Redox states of the mixed-valent pair $\text{Fe}^{\text{II}}\text{Fe}^{\text{III}}$.

MINIREVIEW

oxidation potentials are affected differently, owing to the unsymmetrical charge distribution. The reduction potential of $\{L[(Py)_2][(Py)(BnO)]Fe^{II}(mpdp)Fe^{III}\}^+$ is thus closer to that of $\{L[(Py)(BnO)][(Py)(BnO)]Fe^{III}(mpdp)Fe^{II}\}$ complex than to that of $\{HL[(Py)_2][(Py)_2]Fe^{III}(mpdp)Fe^{II}\}^{2+}$ and the reverse is observed for the oxidation potential. As an immediate consequence, the stability domain of the mixed-valent state is significantly enlarged (see below Section 4.2). Overall, this shows that the two Fe ions do not behave as a redox pair anymore, which is in line with their 1H NMR behavior indicating more localized ions (see above Section 3.5). This independence of the two sites is further evidenced by the behavior of the complex $\{L[(Py)_2][(Py)(Bn)]Fe^{III}(mpdp)Fe^{II}(NCCH_3)\}^{2+}$. When the acetonitrile is replaced by H_2O (Figure 6a), the reduction of the ferric site is weakly affected (-20 mV) as opposed to the oxidation of the ferrous site (-200 mV) (Figure 6b).

4.2. Stability Domains of (μ -Phenoxido) Fe^II/Fe^III Complexes

The stability of the mixed-valent form can be determined from the difference of these electrochemical potentials through the comproportionation constant (Scheme 5). Very different values of $\Delta E_{1/2}$ have been reported for (μ -phenoxido) Fe^II/Fe^III compounds from 560 to 970 mV. For complexes where the lateral branches comprise four N donors, $\Delta E_{1/2}$ values close to 700 mV are observed and this corresponds to comproportionation constants of K_{com} ca $5 \cdot 10^{11}$. When each branch incorporates an anionic O donor, $\Delta E_{1/2}$ becomes close to 600 mV. This ca 100 mV diminution translates into a two orders of magnitude reduction of K_{com} to ca $5 \cdot 10^9$. By contrast, enlarged stability domains are noted for unsymmetrical complexes bearing a single anionic oxygen donor. Depending on its nature (hydroxybenzyl vs phenol), $\Delta E_{1/2}$ extends over 870 to 980 mV, with K_{com} as high as ca $5 \cdot 10^{14}$ to $5 \cdot 10^{16}$, respectively.

On the whole, the stability of mixed-valent form is influenced by diverse factors whose respective weights depend on the nature of the ligands and the bridging pattern.^[73] (i) The structural changes associated to the redox reactions are likely to be minor in the present case of Fe^II/Fe^III couples not involving spin state variations. (ii) The magnetic exchange interactions between the Fe centers are not likely to bring a significant contribution either. As a matter of fact, literature reports show that the exchange interactions of (μ -phenoxido) $FeFe$ complexes are in general less than $|J| \leq 20 \text{ cm}^{-1}$, owing to the fact that phenoxido and carboxylato bridges are modest mediator of antiferromagnetic couplings.^[21] (iii) From a comparison of the mixed-valent Fe^II/Fe^III complex with its Fe^II/Ga^III and Zn^II/Fe^III analogs, Que and coll. estimated that the electronic delocalization contributes ca 100 mV to the stability of the Fe^II/Fe^III species.^[58] (iv) Coulombic interactions are thus appearing as the most important factor as supported by the following observations.

As noted above, $\Delta E_{1/2}$ values close to 700 mV are observed for complexes where the lateral branches comprise four N donors. These values are reduced to ca 600 mV when the bridging carboxylates are replaced by diphenylphosphate whose enlarged bite angle causes a larger Fe-Fe distance (3.64 vs 3.37 Å),^[27,43,52] thereby decreasing the coulombic interactions. Similarly, replacing a neutral pyridine donor by an anionic hydroxybenzyl in each branch lowers by two units the overall charge of the $FeFe$ unit and the coulombic interactions; again $\Delta E_{1/2}$ values lower than 600 mV are noted.^[34,37,74]

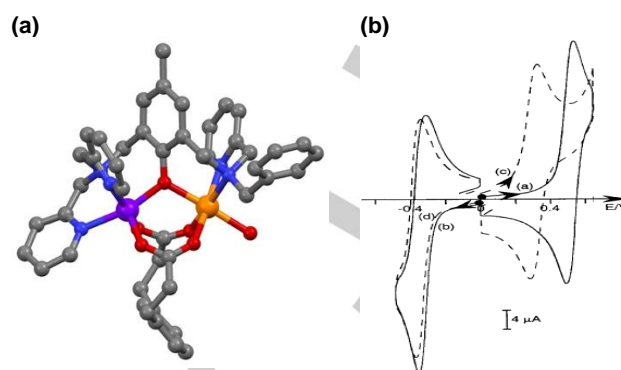


Figure 6. (a) X-ray structure of the cation $\{L[(Py)_2][(Py)(Bn)]Fe^{III}(mpdp)Fe^{II}(OH_2)\}^{2+}$.^[20] (b) Cyclic voltammograms of $\{L[(Py)_2][(Py)(Bn)]Fe^{III}(mpdp)Fe^{II}(NCCH_3)\}^{2+}$ in CH_3CN in absence (solid line) and in presence of 1500 eq H_2O (dashed line).^[62]

5. Electron and Proton Transfers

A few mixed-valent complexes have been isolated with a protic ligand that can undergo deprotonation and some of them exhibit the remarkable behavior of deprotonation-induced valence inversion.^[45,47] As a matter of fact, when the acid form of the complex presents localized valences, deprotonation may lead to an inversion of these valences.

A first piece of evidence was obtained on the $\{L[(Py)_2][(Py)(BnCl_2)]Fe^{III}(mpdp)Fe^{II}(OH_2)\}^{2+}$ complex (Figure 6a) formed upon addition of 1500 molar equiv of water on $\{L[(Py)_2][(Py)(BnCl_2)]Fe^{III}(mpdp)Fe^{II}(NCCH_3)\}^{2+}$.^[62] 1H NMR and Mössbauer spectroscopies evidenced localized valences and the coordination of the water molecule to the ferrous site. When the same amount of water was added on $\{L[(Py)_2][(Py)(BnCl_2)]Fe^{III}(mpdp)Fe^{III}(NCCH_3)\}^{3+}$ generated by bulk electrolysis of the acetonitrile Fe^II/Fe^III complex, Mössbauer spectroscopy evidenced the formation of the aqua complex $\{L[(Py)_2][(Py)(BnCl_2)]Fe^{III}(mpdp)Fe^{III}(OH_2)\}^{3+}$ along with that of the hydroxo complex $\{L[(Py)_2][(Py)(BnCl_2)]Fe^{III}(mpdp)Fe^{II}(OH)\}^{2+}$. A perusal of cyclic voltammograms recorded on the solution of the di-ferric mixture revealed the formation at the electrode of the mixed-valent hydroxo complex. However, this species is unstable towards protonation and is rapidly transformed in the corresponding mixed-valent aqua complex $\{L[(Py)_2][(Py)(BnCl_2)]Fe^{III}(mpdp)Fe^{II}(OH_2)\}^{2+}$. It may be anticipated that the hydroxo ligand was coordinated to the ferric site rather than to the ferrous ion. Accordingly, this hydroxo mixed-valent complex $\{L[(Py)_2][(Py)(BnCl_2)]Fe^{II}(mpdp)Fe^{III}(OH)\}^+$ presented inverted valences versus the aqua complex $\{L[(Py)_2][(Py)(BnCl_2)]Fe^{III}(mpdp)Fe^{II}(OH_2)\}^{2+}$.^[47] The occurrence of such a (de)protonation-induced intervalence charge transfer was fully demonstrated when the ditopic ligand presents an aniline coordinating arm (Figure 7a).^[47] Under the acidic form, the aniline group in $\{L[(Py)_2][(Py)(BnNH_2)]Fe^{III}(mpdp)Fe^{II}\}^{2+}$ is coordinated to the ferrous site as evidenced by X-ray crystallography and Mössbauer spectroscopy. Upon addition of Et_3N , the UV-visible and Mössbauer signatures are fully consistent with the formation

MINIREVIEW

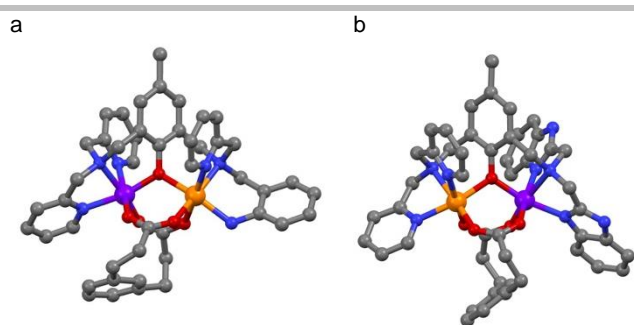


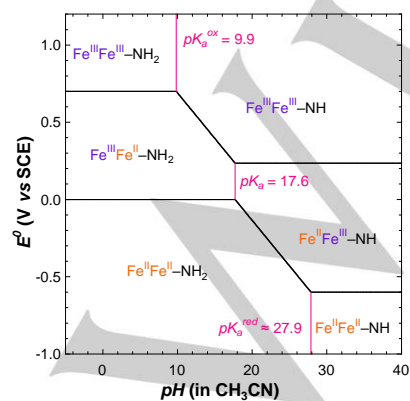
Figure 7. X-ray structures of the cations (a) {[L(Py)₂][(Py)(BnNH)]Fe^{III}(mdp)Fe^{II}}²⁺ and (b) {[L(Py)₂][(BzImH)₂]Fe^{II}(mdp)Fe^{III}}²⁺; mdpH₂ is *m*-phenylene diproionic acid.

of {L[(Py)₂][(Py)(BnNH)]Fe^{II}(mdp)Fe^{III}}⁺ where the anilide ligand is coordinated to the ferric site.

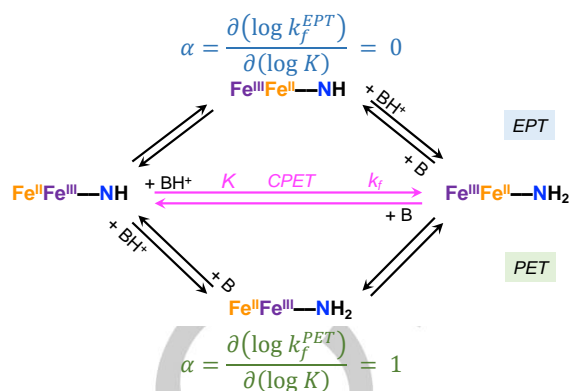
The mechanism of this unprecedented type of proton coupled electron transfer (PCET) was further investigated, in collaboration with the group of J.-M. Savéant,^[25] to discriminate between a concerted process (concerted proton-electron transfer, CPET) and pathways involving two sequential events: either initial electron transfer followed by proton transfer (EPT) or the reverse (PET) (Scheme 6).

A new strategy was devised that relied on determining the dependence of the rate constant (*k_r*) for the formation of one mixed-valent complex from the other (valence inversion) upon the driving force (*K*) of the reaction. The latter can indeed be modified upon using acids and bases possessing different strengths. To access the rate constant *k_r*, it was necessary to rely on a technique allowing (i) to monitor the PCET reaction and (ii) to quantify the distribution of the acidic and basic forms of the mixed-valent complex. Because redox potentials were anticipated to differentiate these two complexes, cyclic voltammetry appeared to be perfectly suited. Moreover, scan rate could be tuned to access the kinetics.

In a first step, the thermodynamics of this system was determined. The Pourbaix diagram was established, thus delineating the pH and potential domains of the aniline and anilide forms of the diferrous, mixed-valent and diferric complexes (See left part of Scheme 7). The *pK_a* values were thus determined for the three oxidation states. As expected, this value increased upon decreasing the redox



Scheme 7. Left: Pourbaix diagram. Middle: Reactions occurring upon reductive scans starting from {[L(Py)₂][(Py)(BnNH)]Fe^{III}(mdp)Fe^{II}}²⁺. The key species and reactions are indicated in bold. Right: Illustration of the scan rate dependence on the 0.0 V redox wave. Adapted from reference ^[25].



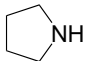
Scheme 6. Middle: Concerted proton-electron transfer (CPET) versus stepwise processes, electron transfer preceding the proton transfer (EPT) or vice versa (PET). Top: Value for the symmetry factor α associated to the EPT process. Bottom: Value for the symmetry factor α associated to the PET process. *k_r* rate of valence inversion, *K* driving force of the reaction. The aniline/anilide ligands are abbreviated by their coordinating functions NH₂/NH⁻. Adapted from ref^[25].

state: 9.9, 17.6 and \approx 27.9 for the Fe^{III}Fe^{III}, Fe^{III}Fe^{II} and Fe^{II}Fe^{II} complexes, respectively.

Triethylamine looked to be a convenient base to investigate the PCET because of its 18.6 *pK_a* value^[75] close to that of the mixed-valent complex. Accordingly, in a second step, cyclic voltammograms were recorded on solutions buffered with a mixture of Et₃N and its conjugated acid Et₃NH⁺ (see middle part of Scheme 7). A pre-electrolysis at 0.4 V vs SCE was performed to generate the {[L(Py)₂][(Py)(BnNH)]Fe^{III}(mdp)Fe^{II}}²⁺ complex at the electrode. Accordingly, a scan in reduction firstly allowed the formation of the {[L(Py)₂][(Py)(BnNH)]Fe^{II}(mdp)Fe^{II}}⁺ complex. Because of the presence of Et₃NH⁺/Et₃N buffer, this anilide complex was further protonated in the quantity dictated by the *K* and *k_r* constants. The formation of {[L(Py)₂][(Py)(BnNH₂)]Fe^{III}(mdp)Fe^{II}}²⁺ was actually assessed by its reduction at 0.0 V vs SCE. Note that {[L(Py)₂][(Py)(BnNH)]Fe^{II}(mdp)Fe^{II}}⁺ was reduced at lower potential values, \approx -0.6 V vs SCE. The simulation of a series of cyclic voltammograms recorded at different scan rates and using different Et₃NH⁺ and Et₃N concentrations, led to the determination of *k_r* (see right part of Scheme 7 and Table 1).

MINIREVIEW

Table 1. Driving force constant and rate constant for the protonation of $\{[L(Py)_2][(Py)(BnNH)]Fe^{III}(mpdp)Fe^{II}\}^+$ using two different bases. Experiments were performed in acetonitrile with 1% of methanol.

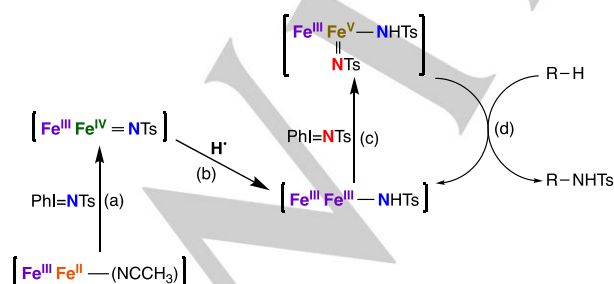
Base	pK_a (in acetonitrile) ^[75]	$\log(K)$	$\log(k)$
Et_3N	18.6	-1	4.5 ± 0.1
	19.6	-2	4.0 ± 0.1

In a third step, analogous experiments were repeated with a stronger base, namely pyrrolidine (see Table 1). A symmetry factor α of 0.5 could be deduced, ruling out the two sequential processes. Lastly, to definitely prove the concerted pathway, experiments were performed to search for a H/D kinetic isotope effect (KIE). Whereas the driving force constant was identical for experiments performed in acetonitrile with 1% of CH_3OH and with 1% of CH_3OD , the rate constant k_f decreased from $3 \cdot 10^4 \text{ M}^{-1} \text{ s}^{-1}$ with CH_3OH down to $1.5 \cdot 10^4 \text{ M}^{-1} \text{ s}^{-1}$ with CH_3OD . A KIE value of 2 was thus deduced that was fully consistent with previous values obtained for CPET reactions.^[76] Hence, combining thermodynamic and kinetic experiments (Pourbaix diagram and cyclic voltammetry) to isotopic H vs D labeling definitely proved that this (de)protonation induced valence inversion occurs as a concerted proton-electron transfer.

6. Hydrogen Atom Abstraction and Tautomerism

6.1. Hydrogen Atom Abstraction

The mixed-valence complex $\{L[(Py)_2][(Py)(Bn)]Fe^{III}(mpdp)Fe^{II}(S)\}(ClO_4)_2$ with $S = H_2O$ or $MeOH$ was designed to present an accessible coordination site on the ferrous site that could be used to promote oxidative reactivities.^[20] As expected, it reacts with tosyliminophenyl iodine to mediate the intramolecular insertion of tosyl nitrene onto the benzyl ortho position.^[22] Moreover, the analog complex $\{L[(Py)_2][(Py)(BnCl_2)]Fe^{III}(mpdp)Fe^{II}(MeOH)\}(ClO_4)_2$ with the two ortho benzylic positions protected by chlorine atoms revealed high catalytic activities in tosyl nitrene transfers to various substrates: thioanisole,^[55] styrene,^[55,77–79] ethylbenzene and cyclohexane.^[24,80] This justified a detailed investigation of the mechanisms of nitrene formation and transfer.



Scheme 8. Summary of redox changes during nitrene formation and transfer to a hydrocarbon. The ^{14}N atom originating from the first iodine reagent ($PhI=^{14}NTs$) is indicated in blue while the ^{15}N isotope from the second iodine reagent ($PhI=^{15}NTs$) is labeled in red.

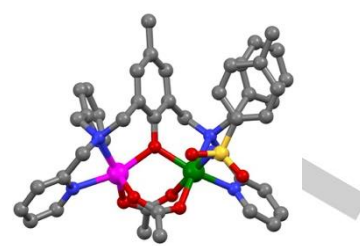


Figure 8. Optimized geometry of the cation $\{L[(Py)_2][(Py)(Bn)]Fe^{III}(MeCO_2)_2Fe^{IV}(NTs)\}^{2+}$. Color code: Fe^{III} in violet and Fe^{IV} in green.

All involved species were identified by a combination of UV-visible and Mössbauer spectroscopies and Desorption ElectroSpray Ionization Mass Spectrometry. In the first step (Scheme 8, reaction (a)) the phenyltosyliodine $PhI=NTs$ reacts with the $[Fe^{III}Fe^{II}]$ complex in a two-electron oxidative addition with elimination of iodobenzene and formation of the mixed-valence $[Fe^{III}Fe^{IV}(=NTs)]$ imido complex. Support for its formation was brought by DFT calculations of the relevant model which revealed that the structural characteristics and Mössbauer parameters of the purported $Fe^{IV}(=NTs)$ entity matched those of well established hexacoordinated Fe^{IV} imido complexes (Figure 8).^[23] In particular the $Fe-N_{Ts}$ distance which amounted to 1.71 \AA is close to that of the reference complex $(N_4Py)Fe^{IV}(NTs)$ ($N_4Py =$ pentanitrogen ligand, 1.73 \AA).^[81] This species is able to catalyze thioanisole sulfimidation and styrene aziridination.^[23] It is also able to abstract a H^\bullet from a H donor (DiHydroAnthracene, or DiPhenylHydrazine) or the ligand benzylic positions (Scheme 8, reaction (b)). This reaction produces the diferric tosylamido $[Fe^{III}Fe^{III}(-NHTs)]$ complex where the diiron center has been reduced by one-electron.^[23,55] The rate of the H^\bullet abstraction reaction was evaluated spectroscopically to ca $6 \text{ M}^{-1} \text{ s}^{-1}$ at $-60 \text{ }^\circ\text{C}$, a value in the range of the most reactive compounds reported by the groups of Sorokin^[82] and Nam.^[83] The electronic structure of the mixed-valence $[Fe^{III}Fe^{IV}(=NTs)]$ imido complex was investigated by detailed DFT computations which unveiled two isoenergetic configurations $[Fe^{III}Fe^{IV}(=NTs)]$ and $[Fe^{III}Fe^{III}(-NHTs)]$. In both, substantial spin density was found on the imido nitrogen. By contrast, none of these configurations possesses spin density on the phenoxido ligand, ruling out a phenoxyl radical. The H^\bullet abstraction ability of the $[Fe^{III}Fe^{IV}(=NTs)]$ imido complex is associated to its high electron affinity ($127.5 \text{ kcal mol}^{-1}$) and the very high value of the $N-H$ bond dissociation energy of the diferric tosylamido $[Fe^{III}Fe^{III}(-NHTs)]$ ($99.7 \text{ kcal mol}^{-1}$).^[23]

The formation of a ferric tosylamido species (Scheme 8, reaction (b)) is a very common degradation process of high valent Fe species and usually a catalytic dead-end. The present system is peculiar in that this diferric species can react again with the iodine (Scheme 8, reaction (c)) in a two-electron oxidative addition to form a higher valent species $[Fe^{III}Fe^V(=NTs)(-NHTs)]$ with both an imido and an amido ligand.^[24] This species is a very powerful nitrene transfer catalyst able to aminate even cyclohexane (Scheme 8, reaction (d)). In addition, it proved the most active in a very recent comparison of non-heme aziridination catalysts.^[79] DFT calculations of the relevant model uncovered that this species is a mixture of two tautomers differing by the coordination of the imido group trans to the phenoxido ligand (Figure 9a) or trans to a pyridine (Figure 9b). Moreover, the

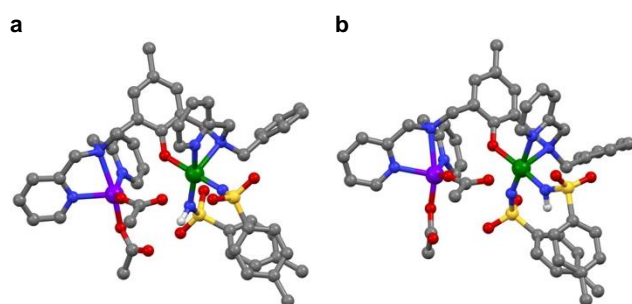


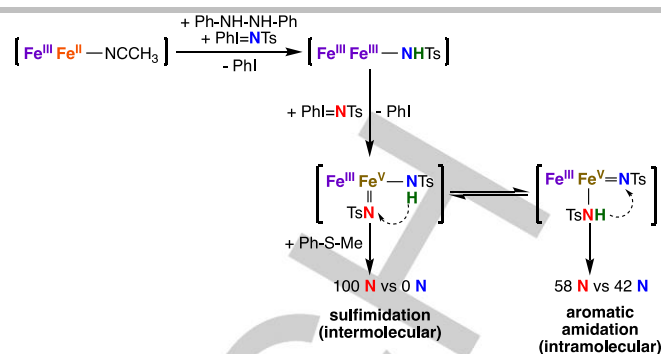
Figure 9. Optimized geometries of the cations (a) trans tautomer $\{L[(Py)_2][(Py)(Bn)]Fe^{III}(MeCO_2)_2Fe^{IV}(NTs)(NHTs)\}^{2+}$ and (b) cis tautomer $\{L[(Py)_2][(Py)(Bn)]Fe^{III}(MeCO_2)_2Fe^{IV}(NHTs)(NTs)\}^{2+}$. Color code: Fe^{III} in violet, Fe^{IV} in green and N-H proton in light gray.

electronic structures of these tautomers differ substantially: that of the trans tautomer is best described as $[Fe^{III}(\mu-PhO)Fe^{IV}(-NTs)(-NHTs)]$ with an imidyl radical trans to the phenoxide while that of the cis tautomer is best described as $[Fe^{III}(\mu-PhO)Fe^{IV}(-NTs)(=NHTs)]$ with an amido ligand trans to the phenoxyl radical. For both tautomers the $Fe-N_{Ts}$ and $Fe-N_{HTs}$ distances, ca 1.8 Å and 1.9 Å respectively, are in the range expected for such compounds. DFT computations revealed that these strongly oxidative properties are due to the very high value of the electron affinity (in particular 142.7 kcal mol⁻¹ for the trans tautomer) associated with the elevated N-H bond dissociation energy of the corresponding bis-tosylamido species $[Fe^{III}Fe^{IV}(-NHTs)_2]$ (95.9 kcal mol⁻¹).

The electronic structures of the two active species deserve to be commented further, in particular with respect to heme proteins. As a matter of fact, both electronic structures of the active amido imido species $[Fe^{III}Fe^{IV}(=NTs)(-NHTs)]$ involve an Fe^{IV} (ligand^{*}) configuration^[24] as cytochrome P450 Compound I.^[84] Likewise, the active imido species $[Fe^{III}Fe^{IV}(=NTs)]$ appears comparable to a Compound II. Notably, the two species reveal similar H^{*} abstraction capacities, in spite of their different oxidative powers illustrated by the different electronic affinities. Actually, the oxidative advantage of $[Fe^{III}Fe^{IV}(=NTs)(-NHTs)]$ over $[Fe^{III}Fe^{IV}(=NTs)]$ is partly compensated by the lower value of the N-H bond dissociation energy of $[Fe^{III}Fe^{IV}(-NHTs)_2]$ vs $[Fe^{III}Fe^{III}-NHTs]$.

6.2. Tautomerism

Compelling experimental evidence for the existence of two tautomeric forms of the active species was obtained through an investigation of nitrene transfer reactions combining ¹⁵N and ²D labeling. To achieve a different labeling of the imido / amido groups, the $[Fe^{III}Fe^{IV}(=NTs)(-NHTs)]$ active species was generated in two steps (Scheme 9): (i) the complex $\{L[(Py)_2][(Py)(Bn)Cl_2]Fe^{III}(mpdp)Fe^{IV}(NCCH_3)\}^{2+}$ was treated with 1 eq. $PhI=^{14}NTs$ in the presence of 1 eq. diphenylhydrazine (H_2DPH), a very good H^{*} donor (BDE(NH) ca 65 kcal mol⁻¹), to generate the amido diferric intermediate, (ii) which was then treated with 1 eq. $PhI=^{15}NTs$ after addition of 10 eq. thioanisole. ESI-MS analysis of the sulfolimine revealed ca 100 % ¹⁵N labeling showing that the second NTs added had been transferred.^[24]



Scheme 9. Tautomeric equilibrium and nitrene transfer.

The same sequence was repeated starting from $\{L[(Py)_2][(Py)(Bn)]Fe^{III}(mpdp)Fe^{IV}(NCCH_3)\}^{2+}$ without added thioanisole to perform the intramolecular amidation of the benzyl group. ESI-MS analysis of the product showed that it had incorporated 58 % ¹⁵N and 42 % ¹⁴N. NTs can be transferred only when in the form of a nitrene (or imido ligand). The initial amido ligand was thus transformed into an imido and the simplest way to explain it is a tautomeric equilibrium. These observations are hence easily rationalized upon considering that NTs transfer to thioanisole is a very fast reaction and occurs before establishment of the tautomeric equilibrium. By contrast, aromatic amidation occurs on a minute time scale^[22] which allows the progression of the tautomeric equilibrium and transfer of both NTs groups. The ¹⁵N/¹⁴N ratio is thus ruled by the competition between the two processes. If the sulfimidation could be slowed down, an increase in the ¹⁴N content should be observed. This was indeed the case when thioanisole was replaced by (*p*-nitro)phenylphenylsulfide. By contrast, an increase in ¹⁵N content should be observed if the establishment of the tautomeric equilibrium could be slowed down, for example by replacement of the exchanged H by a deuterium. This prediction proved true when deuterated diphenylhydrazine (D_2DPH) was used to generate the diferric tosylamido intermediate $[Fe^{III}Fe^{III}(-NDTs)]$, therefore proving the actual presence of tautomeric equilibrium.^[24] This equilibrium is conceptually similar to the oxo-hydroxido equilibrium described by Bernadou and Meunier for manganese porphyrins^[85] and the group of Que for non-heme iron compounds.^[86]

7. Conclusion and Outlook

In this mini-review, we have briefly surveyed the various electron and proton transfers mediated by $(\mu-phenoxido)Fe^{II}Fe^{III}$ complexes. Their complexes with symmetrical ligands (Scheme 1) behave as class II mixed-valent species, indicating that the electronic interaction of the two Fe sites is moderate. As expected, when the ligand is no more symmetrical, the valences of the two Fe ions tend to localize. Central to this review, the localization may be induced by deprotonation of an amine terminal ligand and involve a valence inversion akin to a molecular switch which can be evidenced easily by electronic absorption. This process is an original example of coupled proton and electron transfers and was deciphered by J.-M. Savéant and his colleagues, C. Costentin and M. Robert.

As mentioned, these mixed-valent compounds exhibit very rich spectroscopic and electrochemical properties which have been

MINIREVIEW

used for detection purposes^[40,87] or as tools to investigate catalytic mechanisms.^[13,14] Their strong catalytic potentialities have been especially documented in phosphate ester hydrolysis for which the combination of Fe^{II} binding of substrate and Fe^{III} acidity (to bind a hydroxide ion) has been demonstrated.^[13,14,16,17] They were proved efficient also in nitrene transfer reactions where they allow the generation of very oxidized active species.^[23,24,79] The latter property is no doubt due to the strong stabilization of the Fe^{II} ion by the electrostatic influence of the neighboring Fe^{III} center. This could be used to generate very strong oxidizing agents.

Acknowledgements

The contributions of Dr F. Avenier, Dr S. Chardon-Noblat, Dr M. Clémancey, Dr A. Deronzier, Dr L. Dubois, Dr E. Gouré, Mr J.-F. Jacquot, Mrs. C. Lebrun, Dr P. Maldivi and Dr J. Pécaut are especially acknowledged. Dr P. Maldivi is thanked for critical reading of the manuscript. Partial financial support from the Agence Nationale de la Recherche, Labex Arcane and the Région Rhône-Alpes (Programmes CIBLE) is gratefully acknowledged.

Conflict of Interest

The authors declare no conflict of interest.

Keywords: mixed-valent diiron compound • electron transfer • proton transfer • CPET • tautomerism

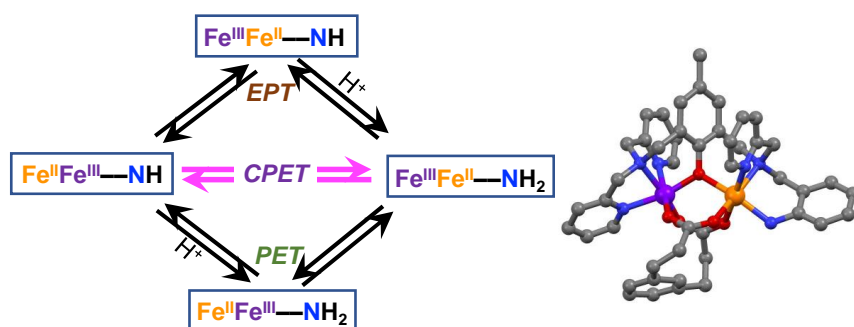
- [1] A. Trehoux, J.-P. Mahy, F. Avenier, *Coord. Chem. Rev.* **2016**, *322*, 142–158.
- [2] A. J. Jasnowski, L. Que Jr., *Chem. Rev.* **2018**, *118*, 2554–2592.
- [3] G. Schenk, N. Mitic, G. R. Hanson, P. Comba, *Coord. Chem. Rev.* **2013**, *257*, 473–482.
- [4] J. M. Bollinger, Y. Diao, M. L. Matthews, G. Xing, C. Krebs, *Dalton Trans.* **2009**, 905–914.
- [5] L. Guddat, A. McAlpine, D. Hume, S. Hamilton, J. de Jersey, J. Martin, *Structure* **1999**, *7*, 757–767.
- [6] Y. Lindqvist, E. Johansson, H. Kaija, P. Vihko, G. Schneider, *J. Mol. Biol.* **1999**, *291*, 135–147.
- [7] N. Sträter, B. Jasper, M. Scholte, B. Krebs, A. Duff, D. Langley, R. Han, B. Averill, H. Freeman, J. Guss, *J. Mol. Biol.* **2005**, *351*, 233–246.
- [8] P. M. Brown, T. T. Caradoc-Davies, J. M. J. Dickson, G. J. S. Cooper, K. M. Loomes, E. N. Baker, *Proc. Natl. Acad. Sci. U. S. A.* **2006**, *103*, 15032–15037.
- [9] G. Schenk, N. Mitic, L. R. Gahan, D. L. Ollis, R. P. McGeary, L. W. Guddat, *Acc. Chem. Res.* **2012**, *45*, 1593–1603.
- [10] W. M. Hussein, D. Feder, G. Schenk, L. W. Guddat, R. P. McGeary, *MedChemComm* **2019**, *10*, 61–71.
- [11] S. Zhou, G. Huang, G. Chen, *Eur. J. Med. Chem.* **2020**, *197*, 112313.
- [12] D. Feder, M.-W. Kan, W. M. Hussein, L. W. Guddat, G. Schenk, R. P. McGeary, *Eur. J. Med. Chem.* **2019**, *182*, 111611.
- [13] P. V. Bernhardt, S. Bosch, P. Comba, L. R. Gahan, G. R. Hanson, V. Mereacre, C. J. Noble, A. K. Powell, G. Schenk, H. Wadeppohl, *Inorg. Chem.* **2015**, *54*, 7249–7263.
- [14] E. Gouré, M. Carboni, A. Troussier, C. Lebrun, J. Pécaut, J.-F. Jacquot, P. Dubourdeaux, M. Clémancey, G. Blondin, J.-M. Latour, *Chem. Eur. J.* **2015**, *21*, 8064–8068.
- [15] W. A. van der Donk, C. Krebs, J. M. Bollinger, *Curr. Opin. Struct. Biol.* **2010**, *20*, 673–683.
- [16] S. J. Smith, R. A. Peralta, R. Jovito, A. Horn Jr., A. J. Bortoluzzi, C. J. Noble, G. R. Hanson, R. Stranger, V. Jayaratne, G. Cavigliasso, L. R. Gahan, G. Schenk, O. R. Nascimento, A. Cavaletto, T. Bortolotto, G. Razzera, H. Terenzi, A. Neves, M. J. Riley, *Inorg. Chem.* **2012**, *51*, 2065–2078.
- [17] P. Comba, L. R. Gahan, V. Mereacre, G. R. Hanson, A. K. Powell, G. Schenk, M. Zajackowski-Fischer, *Inorg. Chem.* **2012**, *51*, 12195–12209.
- [18] G. Xing, Y. Diao, L. Hoffart, E. Barr, K. Prabhu, R. Arner, C. Reddy, C. Krebs, J. Bollinger, *Proc. Natl. Acad. Sci. USA* **2006**, *103*, 6130–6135.
- [19] R. A. Snyder, C. B. Bell, III, Y. Diao, C. Krebs, J. M. Bollinger, E. I. Solomon, *J. Am. Chem. Soc.* **2013**, *135*, 15851–15863.
- [20] W. Kanda, W. Moneta, M. Bardet, E. Bernard, N. Debaecker, J. Laugier, A. Bousseksou, S. Chardon-Noblat, J.-M. Latour, *Angew. Chem. Int. Ed.* **1995**, *31*, 588–590.
- [21] E. Lambert, B. Chabut, S. Chardon-Noblat, A. Deronzier, G. Chottard, A. Bousseksou, J.-P. Tuchagues, J. Laugier, M. Bardet, J.-M. Latour, *J. Am. Chem. Soc.* **1997**, *119*, 9424–9437.
- [22] F. Avenier, E. Gouré, P. Dubourdeaux, O. Sénèque, J.-L. Oddou, J. Pécaut, S. Chardon-Noblat, A. Deronzier, J.-M. Latour, *Angew. Chem. Int. Ed.* **2008**, *47*, 715–717.
- [23] E. Gouré, F. Avenier, P. Dubourdeaux, O. Sénèque, F. Albrieux, C. Lebrun, M. Clémancey, P. Maldivi, J.-M. Latour, *Angew. Chem. Int. Ed.* **2014**, *53*, 1580–1584.
- [24] E. Gouré, D. Senthilnathan, G. Coin, F. Albrieux, F. Avenier, P. Dubourdeaux, C. Lebrun, P. Maldivi, J.-M. Latour, *Angew. Chem. Int. Ed.* **2017**, *56*, 4305–4309.
- [25] R. Balasubramanian, G. Blondin, J. C. Canales, C. Costentin, J.-M. Latour, M. Robert, J.-M. Savéant, *J. Am. Chem. Soc.* **2012**, *134*, 1906–1909.
- [26] M. Suzuki, H. Kanatomi, I. Murase, *Chem. Lett.* **1981**, 1745–1748.
- [27] S. Albedyhl, M. T. Averbuch-Pouchot, C. Belle, B. Krebs, J. L. Pierre, E. Saint-Aman, S. Torelli, *Eur. J. Inorg. Chem.* **2001**, 1457–1464.
- [28] M. Ghiladi, C. McKenzie, A. Meier, A. Powell, J. Ulstrup, S. Wocadlo, *J. Chem. Soc. Dalton Trans.* **1997**, 4011–4018.
- [29] S. Yim, H. Lee, K. Lee, S. Kang, N. Hur, H. Jang, *Bull. Korean Chem. Soc.* **1998**, *19*, 654–660.
- [30] J. Lee, D. J. Jung, H. J. Lee, K. B. Lee, N. H. Hur, H. G. Jang, *Bull. Korean Chem. Soc.* **2000**, *21*, 1025–1030.
- [31] M. Suzuki, A. Uehara, K. Endo, *Inorg. Chim. Acta* **1986**, *123*, L9–L10.
- [32] M. Suzuki, H. Oshio, A. Uehara, K. Endo, M. Yanaga, S. Kida, K. Saito, *Bull. Chem. Soc. Jpn.* **1988**, *61*, 3907–3913.
- [33] M. Mashuta, R. Webb, J. McCluster, E. Schmitt, K. Oberhausen, J. Richardson, R. Buchanan, D. Hendrickson, *J. Am. Chem. Soc.* **1992**, *114*, 3815–3827.
- [34] A. Neves, M. A. Debrito, I. Vencato, V. Drago, K. Griesar, W. Haase, Y. P. Mascarenhas, *Inorg. Chim. Acta* **1993**, *214*, 5–8.
- [35] C. Pathak, M. K. Gangwar, P. Ghosh, *Polyhedron* **2018**, *145*, 88–100.
- [36] V. D. Campbell, E. J. Parsons, W. T. Pennington, *Inorg. Chem.* **1993**, *32*, 1773–1778.
- [37] H. L. Nie, S. M. J. Aubin, M. S. Mashuta, C. C. Wu, J. F. Richardson, D. N. Hendrickson, R. M. Buchanan, *Inorg. Chem.* **1995**, *34*, 2382–2388.
- [38] G. Schwarzenbach, G. Anderegg, R. Sallmann, *Helv. Chim. Acta* **1952**, *35*, 1785–1793.
- [39] A. S. Borovik, B. P. Murch, L. Que, Jr., V. Papaefthymiou, E. Münck, *J. Am. Chem. Soc.* **1987**, *109*, 7190–7191.
- [40] K. Du, E. A. Waters, T. D. Harris, *Chem. Sci.* **2017**, *8*, 4424–4430.
- [41] A. S. Borovik, M. P. Hendrich, T. R. Holman, E. Münck, V. Papaefthymiou, L. Que Jr, *J. Am. Chem. Soc.* **1990**, *112*, 6031–6038.
- [42] M. Suzuki, A. Uehara, H. Oshio, K. Endo, M. Yanaga, S. Kida, K. Saito, *Bull. Chem. Soc. Jpn.* **1987**, *60*, 3547.
- [43] B. Krebs, K. Schepers, B. Bremer, G. Henkel, E. Althaus, W. Müller-Warmuth, K. Griesar, W. Haase, *Inorg. Chem.* **1994**, *33*, 1907–1914.
- [44] C. Belle, I. Gauthier-Luneau, J.-L. Pierre, C. Scheer, E. Saint-Aman, *Inorg. Chem.* **1996**, *35*, 3706–3708.
- [45] E. Gouré, M. Carboni, A. Troussier, P. Dubourdeaux, M. Clémancey, N. Gon, R. Balasubramanian, C. Lebrun, J. Pécaut, G. Blondin, J.-M. Latour, *Inorg. Chem.* **2015**, *54*, 6257–6266.
- [46] B. Battistella, F. Heims, B. Cula, K. Ray, *Z. Anorg. Allg. Chem.* **2020**, *646*, 1010–1019.
- [47] E. Gouré, G. Thiabaud, M. Carboni, N. Gon, P. Dubourdeaux, R. Garcia-Serres, M. Clémancey, J.-L. Oddou, A. Y. Robin, L. Jacquamet, L. Dubois, G. Blondin, J.-M. Latour, *Inorg. Chem.* **2011**, *50*, 6408–6410.
- [48] E. Bernard, W. Moneta, J. Laugier, S. Chardon-Noblat, A. Deronzier, J. Tuchagues, J. Latour, *Angew. Chem. Int. Ed. Engl.* **1994**, *33*, 887–889.
- [49] A. Neves, M. A. Debrito, V. Drago, K. Griesar, W. Haase, *Inorg. Chim. Acta* **1995**, *237*, 131–135.
- [50] C. Belle, G. Gellon, C. Scheer, J.-L. Pierre, *Tetrahedron Lett.* **1994**, *35*, 7019–7022.
- [51] R. Stenkamp, *Chem. Rev.* **1994**, *94*, 715–726.
- [52] K. Schepers, B. Bremer, B. Krebs, G. Henkel, E. Althaus, B. Mosel, W. Müller-Warmuth, *Angew. Chem. Int. Ed. Engl.* **1990**, *29*, 531–533.
- [53] M. A. de Brito, A. Neves, I. Vencato, C. Zucco, V. Drago, K. Griesar,

MINIREVIEW

W. Haase, *J. Braz. Chem. Soc.* **1997**, *8*, 443–446.

- [54] R. Beer, W. Tolman, S. Bott, S. Lippard, *Inorg. Chem.* **1989**, *28*, 4557–4559.
- [55] F. Avenier, J.-M. Latour, *Chem. Commun.* **2004**, 1544–1545.
- [56] L.-J. Ming, H. G. Jang, L. Que Jr., *Inorg. Chem.* **1992**, *31*, 359–364.
- [57] A. S. Borovik, L. Que, Jr., *J. Am. Chem. Soc.* **1988**, *110*, 2345–2347.
- [58] A. S. Borovik, V. Papaefthymiou, L. F. Taylor, O. P. Anderson, L. Que Jr., *J. Am. Chem. Soc.* **1989**, *111*, 6183–6195.
- [59] M. B. Robin, P. Day, *Adv. Inorg. Chem. Radiochem.* **1968**, *10*, 247–422.
- [60] N. S. Hush, *Prog. Inorg. Chem.* **1967**, *8*, 391–444.
- [61] M. Ghiladi, K. Jensen, J. Jiang, C. McKenzie, S. Morup, I. Sotofte, J. Ulstrup, *J. Chem. Soc. Dalton Trans.* **1999**, 2675–2681.
- [62] S. Chardon-Noblat, O. Horner, B. Chabut, F. Avenier, N. Debaecker, P. Jones, J. Pécaut, L. Dubois, C. Jeandey, J.-L. Oddou, A. Deronzier, J.-M. Latour, *Inorg. Chem.* **2004**, *43*, 1638–1648.
- [63] E. Gouré, M. Carboni, P. Dubourdeaux, M. Clémancey, R. Balasubramanian, C. Lebrun, P.-A. Bayle, P. Maldivi, G. Blondin, J.-M. Latour, *Inorg. Chem.* **2014**, *53*, 10060–10069.
- [64] K. Schepers, B. Bremer, B. Krebs, G. Henkel, E. Althaus, B. Mosel, W. Müller-Warmuth, *Angew. Chem. Int. Ed.* **1995**, *29*, 531–533.
- [65] M. Triest, M. J. Davis, C. Reber, *New J. Chem.* **1999**, *23*, 425–432.
- [66] E. P. Day, S. S. David, J. Peterson, W. R. Dunham, J. J. Bonvoisin, R. H. Sands, L. Que, *J. Biol. Chem.* **1988**, *263*, 15561–15567.
- [67] T. Manago, S. Hayami, H. Oshio, S. Osaki, H. Hasuyama, R. Herber, Y. Maeda, *J. Chem. Soc. Dalton Trans.* **1999**, 1001–1011.
- [68] A. Domingo, C. Angeli, C. de Graaf, V. Robert, *J. Comput. Chem.* **2015**, *36*, 861–869.
- [69] Y. Maeda, Y. Tanigawa, S. Hayami, Y. Takashima, *Chem. Lett.* **1992**, 591–594.
- [70] Y. Maeda, Y. Tanigawa, N. Matsumoto, H. Oshio, M. Suzuki, Y. Takashima, *Bull. Chem. Soc. Jpn.* **1994**, *67*, 125–130.
- [71] Y. Maeda, A. Ishida, M. Ohba, S. Sugihara, S. Hayami, *Bull. Chem. Soc. Jpn.* **2002**, *75*, 2441–2448.
- [72] N. Motokawa, S. Hayami, T. Yamamoto, Y. Maeda, *J. Nucl. Radiochem. Sci.* **2006**, *7*, N5–N7.
- [73] R. Gagné, C. Spiro, T. Smith, C. Hamann, W. Thies, A. K. Shiemke, *J. Am. Chem. Soc.* **1981**, *103*, 4073–4081.
- [74] A. Neves, M. A. de Brito, I. Vencato, V. Drago, K. Griesar, W. Haase, *Inorg. Chem.* **1996**, *35*, 2360–2368.
- [75] K. Izutsu, in *Acid-Base Dissociation Constants Dipolar Aprotic Solvents*, Blackwell, Boston, **1990**, pp. 17–35.
- [76] C. Costentin, M. Robert, J. M. Saveant, *Acc. Chem. Res.* **2010**, *43*, 1019–1029.
- [77] R. Patra, G. Coin, L. Castro, P. Dubourdeaux, M. Clémancey, J. Pécaut, C. Lebrun, P. Maldivi, J.-M. Latour, *Catal. Sci. Technol.* **2017**, *7*, 4388–4400.
- [78] G. Coin, R. Patra, M. Clémancey, P. Dubourdeaux, J. Pécaut, C. Lebrun, L. Castro, P. Maldivi, S. Chardon-Noblat, J.-M. Latour, *ChemCatChem* **2019**, *11*, 5296–5299.
- [79] G. Coin, R. Patra, S. Rana, J. P. Biswas, P. Dubourdeaux, M. Clémancey, S. P. de Visser, D. Maiti, P. Maldivi, J.-M. Latour, *ACS Catal.* **2020**, *10*, 10010–10020.
- [80] G. Coin, P. Dubourdeaux, F. Avenier, R. Patra, L. Castro, C. Lebrun, P.-A. Bayle, J. Pécaut, G. Blondin, P. Maldivi, J.-M. Latour, *ACS Catal.* **2021**, *11*, 2253–2266.
- [81] E. J. Klinker, T. A. Jackson, M. P. Jensen, A. Stubna, G. Juhász, E. L. Bominaar, E. Münck, L. Que, *Angew. Chem. Int. Ed.* **2006**, *45*, 7394–7397.
- [82] E. V. Kudrik, P. Afanasiev, L. X. Alvarez, P. Dubourdeaux, M. Clémancey, J.-M. Latour, G. Blondin, D. Bouchu, F. Albrieux, S. E. Nefedov, A. B. Sorokin, *Nat. Chem.* **2012**, *4*, 1024–1029.
- [83] M. S. Seo, N. H. Kim, K. B. Cho, J. E. So, S. K. Park, M. Clémancey, R. Garcia-Serres, J.-M. Latour, S. Shaik, W. Nam, *Chem. Sci.* **2011**, *2*, 1039–1045.
- [84] J. Rittle, M. T. Green, *Science* **2010**, *330*, 933–937.
- [85] J. Bernadou, B. Meunier, *Chem. Commun.* **1998**, 2167–2173.
- [86] M. Puri, A. Company, G. Sabenya, M. Costas, L. Que, *Inorg. Chem.* **2016**, *55*, 5818–5827.
- [87] I. R. W. Z. de Oliveira, A. Neves, I. C. Vieira, *Sens. Actuators B* **2008**, *129*, 424–430.

Table of Contents Graphics



This minireview is a tribute to Prof. J.-M. Savéant who with his group deciphered a deprotonation-induced valence inversion in a $(\mu\text{-phenoxido})\text{Fe}^{\text{II}}\text{Fe}^{\text{III}}$ complex and revealed that it operates through a concerted proton-electron transfer. A survey of the diverse electron and proton transfers exhibited by this family of compounds is presented and sets up the stage of the field.